applied sciences

MDPI

Article

Experimental Activities on a Hydrogen-Fueled Spark-Ignition Engine for Light-Duty Applications

Santiago Molina, Ricardo Novella, Josep Gomez-Soriano * and Miguel Olcina-Girona

CMT—Clean Mobility & Thermofluids, Universitat Politècnica de València, Camino de Vera s/n, 46022 Valencia, Spain; samolina@mot.upv.es (S.M.); rinoro@mot.upv.es (R.N.); miolgi@mot.upv.es (M.O.-G.)
* Correspondence: jogoso1@mot.upv.es

Abstract: The increase in the overall global temperature and its subsequent impact on extreme weather events are the most critical consequences of human activity. In this scenario, transportation plays a significant role in greenhouse gas (GHG) emissions, which are the main drivers of climate change. The decline of non-renewable energy sources, coupled with the aim of reducing GHG emissions from fossil fuels, has forced a shift towards a net-zero emissions economy. As an example of this transition, the European Union has set 2050 as the target for achieving carbon neutrality. Hydrogen (H_2) is gaining increasing relevance as one of the most promising carbon-free energy vectors. If produced from renewable sources, it facilitates the integration of various alternative energy sources for achieving a carbon-neutral economy. Recently, interest in its application to the transportation sector has grown, including different power plant concepts, such as fuel cells or internal combustion engines. Despite exhibiting significant drawbacks, such as low density, combustion instabilities, and incompatibilities with certain materials, hydrogen is destined to become one of the future fuels. In this publication, experimental activities are reported that were conducted on a spark-ignition engine fueled with hydrogen at different operating points. The primary objective of this research is to gain a better understanding of the thermodynamic processes that control combustion and their effects on engine performance and pollutant emissions. The results show the emission levels, performance, and combustion characteristics under different conditions of dilution, load, and injection strategy and timing.

Keywords: hydrogen fuel; combustion; hydrogen engine; clean transportation

check for updates

Citation: Molina, S.; Novella, R.; Gomez-Soriano, J.; Olcina-Girona, M. Experimental Activities on a Hydrogen-Fueled Spark-Ignition Engine for Light-Duty Applications. *Appl. Sci.* **2023**, *13*, 12055. https://doi.org/10.3390/app132112055

Academic Editor: Jun Cong Ge

Received: 16 October 2023
Revised: 30 October 2023
Accepted: 3 November 2023
Published: 5 November 2023

Copyright: © 2023 by the authors. Licensee MDPI, Basel, Switzerland. This article is an open access article distributed under the terms and conditions of the Creative Commons Attribution (CC BY) license (https://creativecommons.org/licenses/by/4.0/).

1. Introduction

Hydrogen stands out as one of the alternatives in the pursuit of decarbonizing the automotive sector due to its carbon-free composition, making it a compelling choice for curbing greenhouse gas (GHG) emissions [1]. The EURO VII regulation, designed for the future, not only targets the reduction in nitrogen oxide (NO_x) emissions but also proposes a significant reduction in carbon dioxide (CO_2) emissions from vehicle fleets. Specifically, it aims to achieve a 15% reduction from 2021 levels by 2025 and an even more ambitious goal of up to 37.5% by 2030. For light-duty vehicles, the targets are set at 15% and 31%, respectively [2].

Various methods exist for hydrogen production, with green hydrogen being a noteworthy example. Green hydrogen is generated through electrolysis powered by renewable energies and is deemed a crucial component of the broader effort to decarbonize the economy [3,4]. Beyond its role as a potential fuel for the automotive sector, hydrogen is also being explored as an energy vector to manage the variable energy outputs from renewable sources [5]. However, it is important to note that the majority of hydrogen currently originates from fossil resources. The predominant method of production is steam methane reforming (SMR) [6], a process that contributes to GHG emissions by releasing carbon in the form of CO_2 into the atmosphere. To mitigate this environmental impact, efforts are

underway to integrate carbon capture mechanisms into SMR production [7]. Nevertheless, carbon capture technology remains an ongoing subject of research and development.

Hydrogen can find various applications within the automotive industry, primarily in two ways: it can be employed in fuel cells (FCs) or in internal combustion engines (ICEs). FC vehicles boast impressive tank-to-wheel efficiencies, hovering around 50% [8], and produce zero NO_x emissions, emitting only water vapor (H_2O) as exhaust. Despite these advantages, the dynamic behavior of FC systems in automotive applications poses challenges, significantly reducing the durability of FC stacks [9] and leading to catalyst corrosion. Some well-established engine manufacturers, including Toyota, Honda, and Hyundai, have already introduced commercial FC vehicles. However, the production cost remains high, partly due to the lack of economies of scale [8]. Nevertheless, the reliance on batteries to distribute energy generated by the FC stack comes with its drawbacks, such as the involvement of rare-earth elements and battery degradation, akin to those of battery electric vehicles (BEVs).

On the other hand, when hydrogen is applied to ICEs [10], it exhibits a higher tolerance for purity, reduces the use of rare-earth materials, and allows for a relatively straightforward adaptation of existing engine models to replace conventional carbon-based fuels [11]. This adaptability makes this technology a compelling option for the future of the carbon-free automotive sector [12]. Also, the absence of carbon virtually eliminates unburned hydrocarbons (HC), carbon monoxide (CO), and CO_2 emissions, with these pollutants being generated only in very small proportions through the combustion of lubricant in the combustion chamber [13].

Recent research efforts have concentrated on adapting engine designs to leverage the unique properties of hydrogen, entailing modifications in fuel supply, combustion chambers, and ignition systems to ensure safety and efficiency. Safety concerns stemming from hydrogen's low ignition energy and wide flammability range have prompted research into secure handling and storage, especially in vehicle applications [14]. Beyond engine adjustments, efforts have been directed towards broader infrastructure considerations, including hydrogen production, transportation, and distribution for widespread use [15]. The ongoing research is also focused on advancements in materials science, catalyst development, and general engine technology to enhance hydrogen compatibility as a fuel in spark-ignition engines.

In this context, the primary focus in hydrogen internal combustion engines (H_2-ICEs) is on reducing NO_x emissions [16]. The formation of nitrogen oxide (NO) can be attributed to thermal, prompt, and fuel mechanisms. The thermal NO_x mechanism develops under high temperatures, the prompt NO_x mechanism is activated at low temperatures in the early combustion stages, and the fuel NO_x mechanism depends on the fuel composition [17]. In the case of hydrogen, the absence of nitrogen renders the fuel NO_x mechanism irrelevant, with the thermal path being the most pertinent one [18–20].

The properties of hydrogen facilitate stable combustion with high dilution, leading to a decrease in the concentration of the generated NO_x [21]. It is widely acknowledged that when the air-to-fuel equivalence ratio (λ) exceeds two [13,22], these emissions are notably diminished. Nevertheless, the challenges associated with NO_x emissions during transient operating conditions (i.e., dynamic torque build-up phases) became evident in several investigations [23]. During these transitional periods, it is common for the air path system to experience delays in the boost pressure, resulting in a reduced air-to-fuel ratio and, consequently, brief NO_x emission spikes. Consequently, selective catalytic reduction (SCR) must be implemented to mitigate these emissions [24]. Recent research has explored the use of hydrogen as a reducing agent in SCR systems. The availability of onboard hydrogen represents an innovative and convenient approach to NO_x reduction, eliminating the need for urea/NH_3 storage in tanks and the potential event of ammonia slip at the tailpipe. The results of using H_2-deNO_x catalysts are promising in reducing NO_2 at low temperatures under lean combustion conditions [25].

Despite these advancements, there is still a significant gap to fill, such as finding the relationship between GHG emissions and pollutants (i.e., NO_x), as well as establishing the limits that minimize both. This study strives to enhance the current understanding of the impacts of mixture formation by employing diverse operating strategies. Its objective is to aid in the progression of contemporary technology for the integration of hydrogen as a fuel in small road transportation solutions. An extensive experimental campaign using a single-cylinder spark-ignition (SI) research engine was conducted to evaluate performance, combustion processes, and emissions. The analysis included scenarios in which the engine was equipped with both port fuel injection (PFI) and direct injection (DI) [26] systems under varying degrees of air dilution and ignition timing.

2. Materials and Methods

Engine Architecture and Test Cell Characteristics

The experiments were conducted using a single-cylinder SI engine with a displacement of 454.2 cm^3. These experimental facilities were previously employed in research conducted by Molina et al. [27,28]. For reference, the key specifications of the engine are provided in Table 1. The engine has an 86 mm stroke, a compression ratio (CR) of 10.7:1, and a 4-valve pent-roof cylinder head. All the experimental tests utilized a conventional spark plug ignition system. Two different injection systems were used for the fuel supply: one being a PFI system capable of a maximum injection pressure of 5 bar, and the other a medium-pressure DI injection system with a maximum pressure of 30 bar. The DI system was specifically designed to enable a brief injection duration, ensuring the precise delivery of the necessary fuel quantity as the injection moved closer to the top dead center (TDC). The control of the fuel injected was managed by regulating the injection duration as a pivotal parameter. The hydrogen was stored and supplied in pressurized tanks at 200 bar.

The engine was installed in a fully instrumented test cell, designed as illustrated in Figure 1. The initial test bench layout, originally intended for gasoline as fuel, was adapted for the use of pure hydrogen. Previous research included investigations into CNG and HCNG dual fuel systems [28]. For safety measures, an intake manifold flame arrester was installed upstream of the EGR mixer, and a dedicated hydrogen supply system was implemented to provide fuel to the injectors.

Table 1. Main engine specifications.

Number of cylinders	1
Number of strokes	4
Displaced volume	454.2 cm^3
Stroke	86.0 mm
Injection systems	PFI/DI
Ignition system	Spark plug
Cylinder diameter	82.0 mm
Compression ratio	10.7
Connecting rod length	144.0 mm
Valves per cylinder	2 intake, 2 exhaust
Engine management system	AVL PREMS GDI
Combustion system	4-valve pent-roof GDI
Intake valve opening (IVO) *	−380 CAD
Intake valve closing (IVC) *	−135 CAD
Exhaust valve opening (EVO) *	−600 CAD
Exhaust valve closing (EVC) *	−338 CAD

* with respect to the firing TDC (0 CAD).

The experimental facility offers comprehensive control over each relevant parameter during engine operation. High-diluted air conditions were achieved using an external compressor, while exhaust back-pressure control was maintained through a knife-gate valve situated in the exhaust line. Automated valves were employed to manage the hydrogen injection pressure when transitioning between the PFI and DI modes.

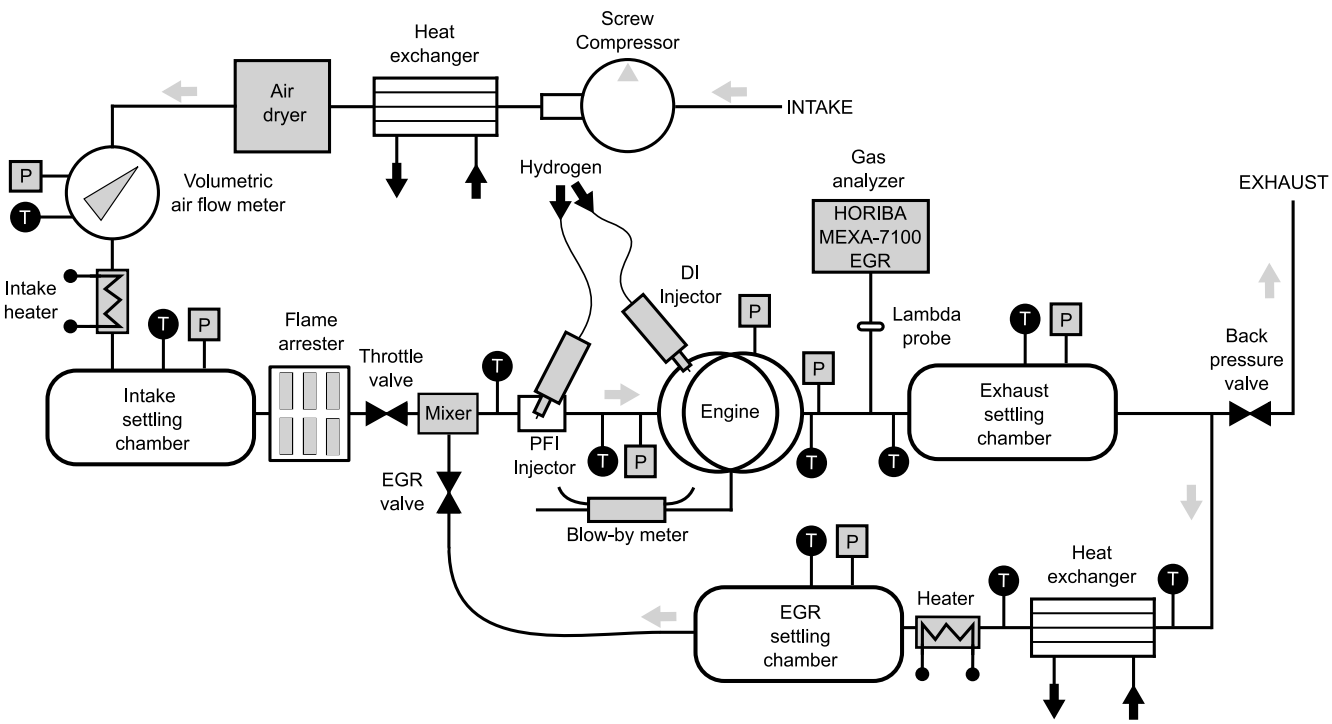

Figure 1. Experimental engine layout.

The test bench was fully equipped with state-of-the-art measurement devices. In-cylinder pressure was measured using a piezoelectric sensor, while the intake and exhaust pressures were monitored using two distinct piezoresistive sensors. A Bronkhorst F-113AC-1M0-AAD-55-V flowmeter was employed to record the hydrogen flow rate. Three distinct methods were employed to measure and estimate the air-to-fuel ratio: an exhaust gas analyzer, an λ sensor positioned at the exhaust tailpipe, and consideration of the various flows within the intake manifold (comprising air and fuel). All signals were captured at a sampling frequency of 0.2 CAD. For the analysis of NO_x emissions and other relevant exhaust gases, HORIBA MEXA-7600EGR equipment was utilized. Table 2 provides an overview of the instrumentation along with its corresponding accuracy.

Hydrogen exhibits highly specific combustion properties suitable for internal combustion engines, and the most significant properties are summarized in Table 3. Notably, it possesses a wide ignition range in air, spanning from 4 to 73% by volume, allowing for stable combustion even with extremely lean mixtures. Furthermore, hydrogen boasts a high combustion speed of approximately 230 cm/s with a stoichiometric mixture, which is five times higher than that of conventional fuels. However, its low density and higher air-to-fuel ratio do reduce the volumetric efficiency in PFI applications. The fuel used in the experimental campaign boasted a purity of 99.9%, with the main impurities being H_2O at $\leq$40 ppm and O_2 at $\leq$10 ppm.

For the analysis of combustion, a diagnostic tool [29] was employed to estimate the combustion-related parameters, including the indicated mean effective pressure (IMEP), the cycle-to-cycle variability (CCV) represented by the coefficient of variation of the IMEP (COV_{IMEP}), the heat release rate (HRR), and combustion-related metrics, such as the combustion phasing (CA50), the combustion onset (CA10), and the end of combustion (CA90). This combustion diagnostic tool calculates the energy released during combustion with certain simplifying assumption, solving the energy equation based on the measured in-cylinder pressure. It takes into account factors such as the uniform pressure and temperature distributions throughout the combustion chamber, as well as various simplifications for estimating the heat transfer to the cylinder walls.

Table 2. Instrumentation accuracy.

Signal (High Frequency)	**Sensor**	**Specification**
In-cylinder pressure	Piezoelectric sensor	0 to 250 bar ± 0.3% linearity
Intake pressure	Piezoresistive sensor	0 to 10 ± 0.001 bar
Exhaust pressure	Piezoresistive sensor	0 to 10 ± 0.001 bar
Variable (Low Frequency)	**Sensor**	**Specification**
Engine speed	Optical angular encoder	1 to 6000 ± 1 rpm
Engine torque	Strain-gauges torque-meter	−200 to 200 ± 1 N m
Intake pressure	Piezoresistive transducer	0 to 10 bar ± 1%
Exhaust pressure	Piezoresistive transducer	0 to 10 bar ± 0.3%
Intake temperature	Thermocouple type K	0 to 1000 ± 0.5 °C
Exhaust temperature	Thermocouple type K	0 to 1000 ± 0.5 °C
Fluid temperature	Pt100 thermoresistance	−200 to 850 ± 0.3 °C
Air mass flow	Air flow meter	0.6–100 m^3/h ± 1%
Hydrogen mass flow	Thermal mass flow meter	N_2 200–1600 L/min ± 0.5 %
Pollutant/Analyzer	**Range**	**Accuracy**
HC/FID	min. 0 to 10 ppm C max. 0 to 50 kppm C	±3%
NO_x/CLD	min. 0 to 10 ppm max. 0 to 10 kppm C	±3%
CO/NDIR	min. 0 to 3 kppm C max. 0 to 12 vol%	±3%
CO_2/DIR	min. 0 to 5 kppm C max. 0 to 20 vol%	±3%
O_2/PMA	min. 0 to 5 vol% max. 0 to 25 vol%	±3%

Table 3. H_2 properties.

RON	>130
AF_{st}	34.3
LHV	119.9 MJ/kg
Molar mass	2.01 g/mol
Purity	≥99.9%

3. Methodology

The methodology employed in this investigation aimed to assess hydrogen combustion under various operating conditions and injection systems in an SI research engine. For this research, a multitude of data points were collected to determine the most significant effects on the hydrogen combustion engine parameters.

The experimental campaign encompassed three distinct load conditions, representing key areas within the operating map, all at an engine speed of 1500 rpm [30]. To determine the load for these operating points, the quantity of injected hydrogen was utilized. Two injector systems were utilized: PFI and DI. For PFI, a wide range of λ values was measured (from 1.4 to 4.0), whereas for DI, measurements were taken from 2.2 to 3.4. Additionally, for each data point, a sweep of the start of injection (SOI) was performed to analyse the impact of the injection timing. To mimic realistic boosting conditions, the exhaust back-pressure was carefully regulated, maintaining a 0.1 bar difference between the intake and exhaust pressures. Table 4 presents a summary of the tests conducted for this investigation.

The experimental data were collected following a testing protocol similar to the one described in reference [27]. To minimize measurement uncertainties, each test was repeated three times. The results presented in the following sections represent the average values of the parameters under study.

Table 4. Details of the experimental tests carried out in this investigation.

Engine Speed [rpm]	Hydrogen [mg/str]	λ	Injection System
1500	4.96	[1.4:0.2:4.0]	PFI/DI
1500	8.08	[2.4:0.2:3.4]	PFI/DI
1500	10.92/11.37	2.6/1.8	PFI/DI

4. Results and Discussion

This section presents the results of the experimental campaign, which are divided into three sections. Each section offers a concise description of the main findings, highlights relevant trends, and provides interpretations of the involved phenomena.

4.1. Effects of Air Dilution

Initially, we delve into the outcomes pertaining to the air dilution effect. This parameter holds a position of utmost importance within the realm of engine parameters. The scientific literature extensively attests to the merits of lean combustion, encompassing the reduction in thermal losses, NO_x emissions, and decreased susceptibility to knock, among other advantages. This acquires heightened significance in the context of hydrogen-fueled engines due to hydrogen's remarkable combustion properties, facilitating the achievement of ultra-lean combustion while maintaining burning stability.

Figure 2 depicts the cycle-averaged profiles of the in-cylinder pressure and heat release rate (HRR). These profiles were obtained from the low-load operating point (4.96 mg/str H_2) at 1500 rpm as the dilution rate was increased. The achievement of conditions for maximum brake torque (MBT) involved spark timing optimization. For this purpose, the characterization of the air dilution was accomplished through the air-fuel equivalence ratio parameter (λ) using the PFI system.

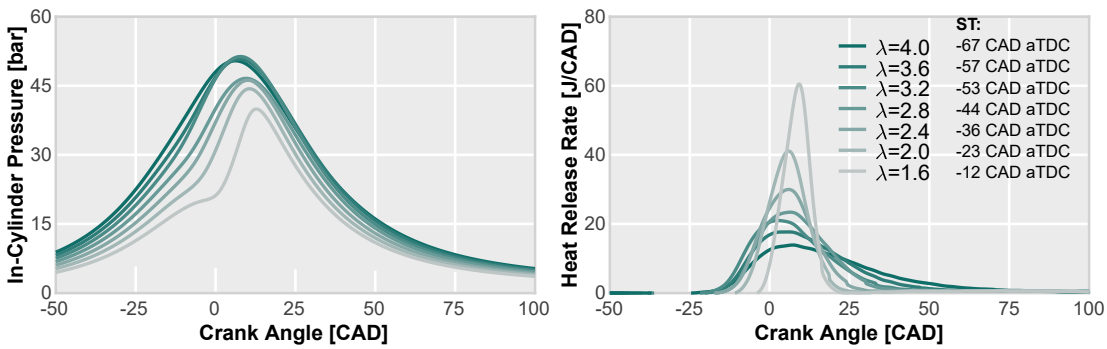

Figure 2. In-cylinder pressure and HRR profiles at 1500 rpm engine speed and low-load conditions, obtained using the PFI system, showcasing variations with different λ values under the MBT conditions.

In these results, it is evident that higher λ values correspond to elevated pressure profiles. With the fuel quantity held constant, increasing λ necessitates an increased intake pressure when using a PFI system. The high values, which reach almost 1.8 bar even under these low load conditions, were necessary to sustain the dilution conditions when using hydrogen as a fuel, especially at high values of λ (>2), to restrict the operation of PFI-based engines at high load conditions due to boosting system limitations or maximum in-cylinder pressure peaks. The impact on the HRR profiles reveals that as the dilution increases, the curve flattens and widens. The extended duration of combustion is attributed to deteriorated combustion propagation conditions.

These trends are more effectively illustrated in Figure 3, where the maximum in-cylinder pressure and the HRR peaks are displayed alongside the pertinent combustion periods as the dilution rate varies. As can be observed, this figure reaffirms the previously noted observation, showcasing a rising trend in the in-cylinder pressure peaks with λ. Notably, at λ = 4, combustion instabilities impact the average pressure profile, resulting in

a reduction in the maximum peak value due to unburned cycles and partial combustion. This cyclic variation establishes the stability limit for air dilution.

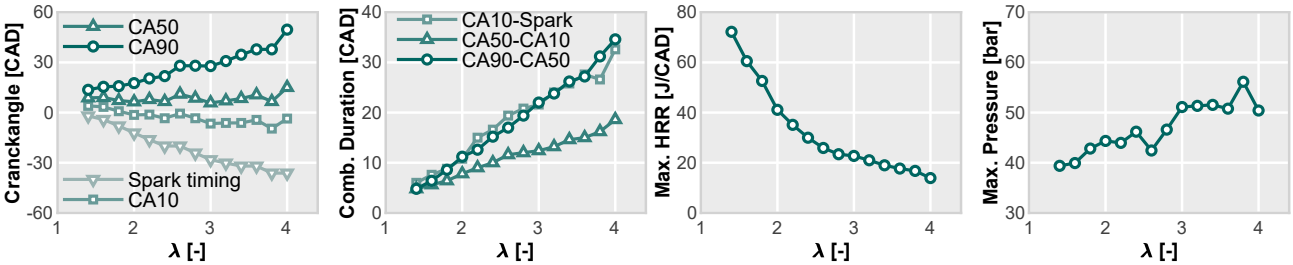

Figure 3. Maximum in-cylinder pressure and HRR peaks, characteristic combustion periods (CA10, CA50, and CA90), spark timing, combustion duration periods (CA-Spark timing, CA50-CA10, and CA90-CA10) obtained at 1500 rpm engine speed and low-load conditions for various λ values. Combustion phasing was optimized to achieve MBT conditions, and the results were obtained using the PFI system.

As illustrated in Figure 2, the results in Figure 3 also corroborate that the maximum HRR value decreases as more diluted conditions are reached. This decline in the HRR peaks exhibits two distinct slopes: an initial region where increasing dilution significantly reduces the maximum peaks, particularly up to $\lambda \approx 2.6$, and a subsequent region where further dilution exerts less influence, albeit still leading to a decrease in the maximum value.

Figure 3 also presents crucial combustion parameters, encompassing the combustion phasing and duration. Under MBT conditions, the combustion phasing (CA50) falls within the approximate range of 8 to 10 CAD. It is noteworthy that CA10 experiences only marginal effects from increasing λ, whereas CA90 exhibits a significant dependency on λ, rising from approximately 15 CAD to values surpassing 30 CAD.

Additionally, the duration of different combustion phases, derived from the aforementioned parameters, are also depicted in Figure 3. CA50-10 displays the least sensitivity to air dilution, characterized by the smallest slope. Both the end of combustion (CA90-50) and the combustion initiation (spark timing-CA10) are equally influenced, demonstrating identical slopes and initial values.

The impact of λ on the engine performance and emissions is illustrated in Figure 4. These figures depict the results for both low-load and mid-load conditions (8.08 mg/str H_2). The results presented here were obtained using the PFI injection system, and they represent the optimal combustion phasing or MBT.

For the low-load point, the following trends emerge. Instabilities, as indicated by COV_{IMEP}, begin to increase more steeply at around $\lambda = 3.2$. The specific fuel consumption reaches its minimum value at $\lambda = 3.2$, coinciding with the air dilution ratio that maximizes the engine performance and efficiency. At this point, the engine achieves an IMEP of 5.2 bar, corresponding to 40% of the gross indicated efficiency (GIE).

For the mid-load point, the operating range for dilution spans from $\lambda = 2.4$ to 3.4. The lowest achievable dilution value is $\lambda = 2.4$. Higher dilutions are necessary to reduce the risk of abnormal combustion (knocking), which can lead to engine damage, especially considering the higher pressure and temperatures reached in the combustion chamber. The engine performance starts to decline when the air dilution equivalence ratio exceeds 3.4, consistent with the trend observed at low-load conditions. At $\lambda = 3$, a peak in GIE and IMEP is observed. This trend holds true for both low- and mid-load conditions, where the combustion process becomes less efficient as λ increases. The minimum specific fuel consumption drops below 74 g/kWh, with an efficiency and engine performance improvement, with IMEP exceeding 8.7 bar.

In earlier studies, it was observed that NO_x emissions peaked at $\lambda = 1.3$ [13]. Values above 2 significantly reduce this pollutant by impeding the thermal formation mechanism. The results obtained in this investigation are consistent with previous findings, notably

reducing its value for $\lambda > 2$. In the case of mid-load conditions, due to limitations related to engine knock, the first λ value that ensures safe operation brings NO_x emissions levels below 1 g/kWh. However, although higher dilution can minimize NO_x emissions stemming from the thermal mechanism, they never reach zero because other formation pathways persist.

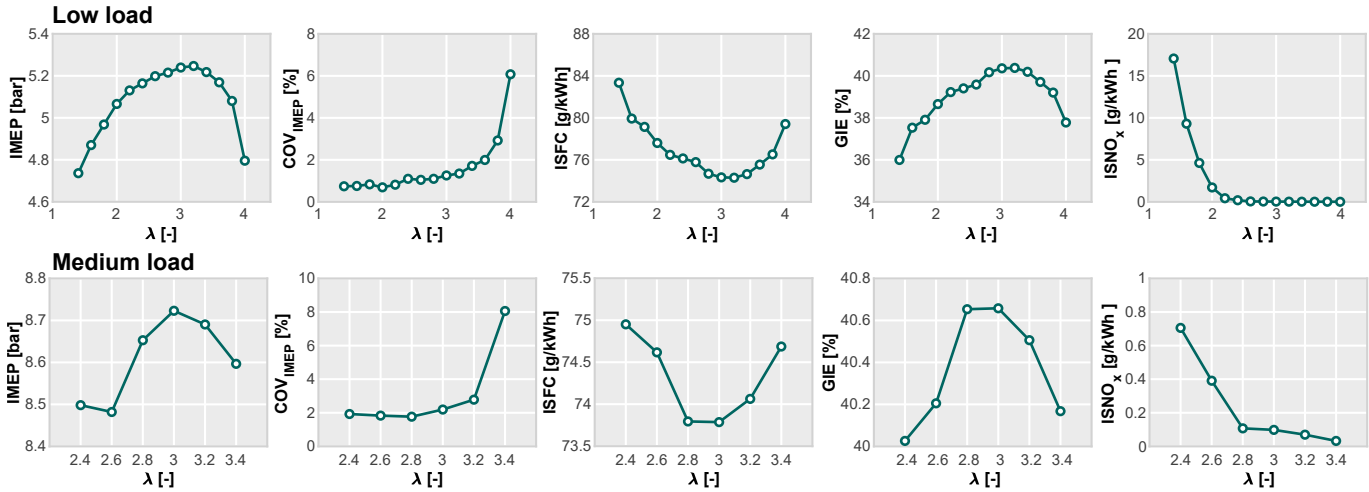

Figure 4. IMEP, gross indicated efficiency (GIE), COV_{IMEP}, indicated specific fuel consumption (ISFC), and indicated specific NO_x emissions at 1500 rpm engine speed, under both low- and mid-load conditions, with varying λ. Combustion phasing was optimized to achieve MBT conditions. Results obtained using the PFI system.

During engine operation, certain limitations reported in the literature on PFI-based H_2-engines were identified. Figure 5 includes all the measured data points to provide an overview of the operational limits as a function of the air dilution and engine load.

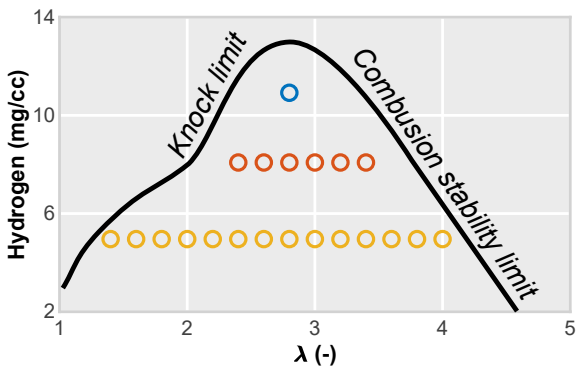

Figure 5. Schematic illustrating the operational limits of dilution using the PFI engine configuration.

The available engine operating region is constrained by two primary factors that affect the performance and efficiency. The knocking tendency increases as the quantity of the injected hydrogen rises and the level of dilution decreases, whereas the combustion stability is compromised mainly due to dilution. With an increase in the quantity of fuel, the effective range of λ decreases. Additionally, elevated in-cylinder pressure and temperature increase the likelihood of knocking and intensify its impact. Conversely, combustion stability due to an excessively diluted mixture can lead to abnormal combustion phenomena, such as pre-ignition, backfire, or even knocking. When the mixture fails to burn completely, a portion of the hydrogen remains inside the cylinder, reducing the effective λ. This can result in extremely fast combustion or the pre-ignition of gases during both the intake and compression strokes.

The optimal performance zone, regardless of the quantity of hydrogen, was found to be within the range of λ values between 2.5 and 3.2. In terms of emissions, low levels of NO_x are obtained within this dilution range. Thus, operating the engine within this dilution range can maximize the performance while minimizing pollutant emissions. However, increasing dilution up to these levels requires a suitable boosting system capable of delivering the necessary pressure and air volume. Additionally, transient events may lead to high NO_x emissions and increase the risk of entering a high-knock-tendency condition, potentially causing damage to the engine.

4.2. Sensitivity to Combustion Phasing

Another important parameter is the spark timing, which allows for controlling the combustion phasing. The sensitivity of combustion to this parameter is of utmost relevance, as it can enhance the flexibility of control strategies, improve vehicle driveability, optimize the functioning of the after-treatment system, and reduce costs related to its design and packaging.

In Figure 6, the in-cylinder pressure and heat release profiles are depicted for a spark timing sweep at the low-load point, corresponding to two different dilution conditions. As the spark timing is advanced, the pressure profiles rise and move in the direction of the compression stroke, irrespective of the λ value. When analyzing the heat release rate profiles, a similar trend parallel to the pressure profiles is observed; they advance as the spark timing moves towards the compression stroke, becoming slightly narrower and displaying higher peak values.

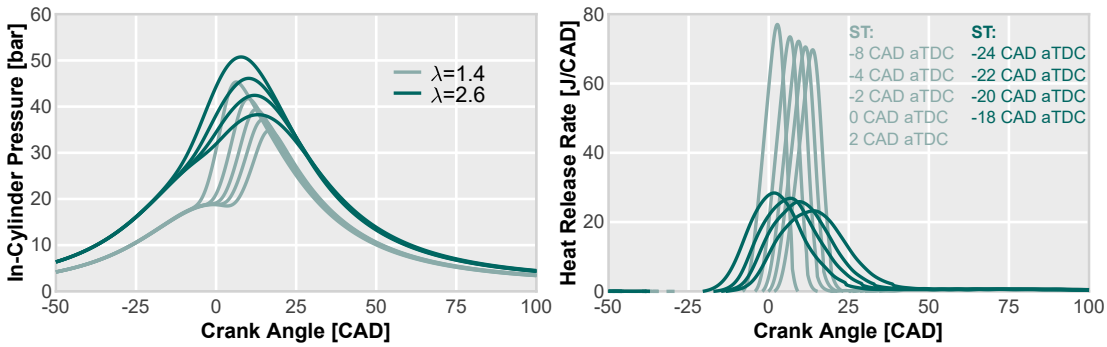

Figure 6. In-cylinder pressure and HRR profiles at 1500 rpm engine speed and low-load conditions, obtained using the PFI system, showcasing variations with different spark timing values for two dilution conditions.

By expanding the range of λ values (as shown in Figure 7), we can confirm the trends described earlier. The spark timing plays a crucial role in controlling the combustion phasing, as evident from the linear trends depicted in Figure 7. As λ increases, the influence of the spark timing on the combustion phasing becomes more pronounced, making precise control challenging. Even minor adjustments in the spark timing can lead to significant changes in the combustion phasing. Additionally, it becomes clear that maintaining the desired combustion phasing as λ increases necessitates advancing the spark timing.

Figure 8 displays the primary engine parameters for the same conditions as shown in Figure 7. Concerning the engine performance, one can observe that the trends become flatter as λ increases. However, the range within which the combustion remains stable becomes more limited as the dilution increases. For instance, in the case of λ = 1.4, there is no discernible effect of the spark timing on the combustion stability. Nevertheless, COV_{IMEP} rapidly increases with spark timing variations at λ = 2.6.

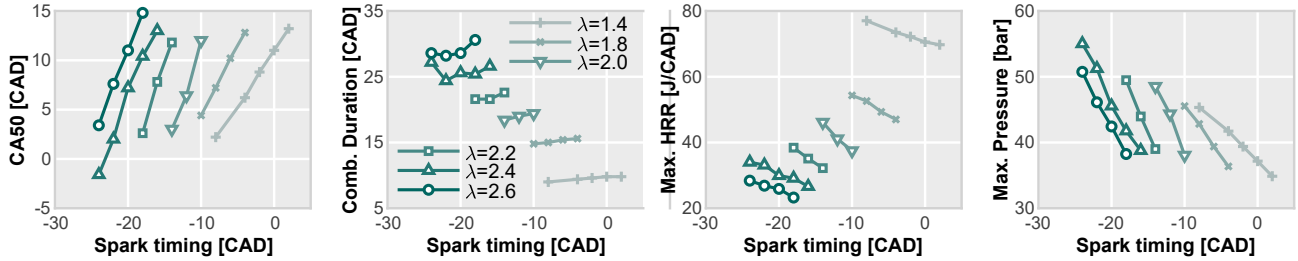

Figure 7. Maximum in-cylinder pressure and HRR peaks, characteristic combustion periods (CA10, CA50, and CA90), spark timing, combustion duration periods (CA-Spark timing, CA50-CA10, and CA90-CA10) obtained at 1500 rpm engine speed and low-load conditions for various spark timing values. The results were obtained using the PFI system and multiple dilution conditions.

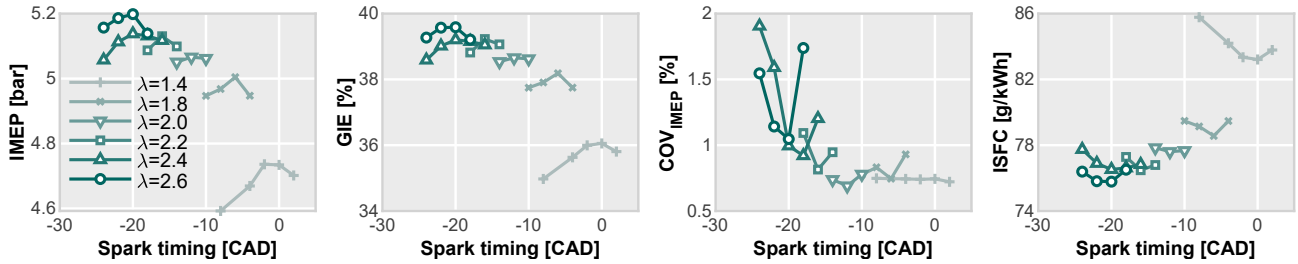

Figure 8. IMEP, GIE, COV_{IMEP} and ISFC at 1500 rpm engine speed, under low-load conditions and different spark timings. Results obtained using the PFI system.

Traditionally, spark timing has also been employed to delay combustion in order to control NO_x emissions. However, the influence of the spark timing on these emissions is minimized under lean combustion conditions, as illustrated in Figure 9. Lower local temperatures inhibit the NO_x thermal formation mechanism, thereby diminishing the impact of delayed combustion.

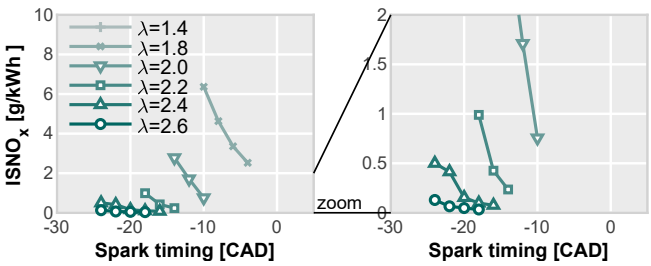

Figure 9. $ISNO_x$ emissions at 1500 rpm engine speed, under low-load conditions and different spark timings. Results obtained using the PFI system.

4.3. Effects of Injection Strategy

In this section, a comparison is conducted between the PFI and DI injection systems with the objective of identifying and understanding the potential differences in terms of performance and emissions. To do this, the analysis focuses on the low-load point, where the injection system has been switched to DI while maintaining the amount of hydrogen. Initially, the start of injection (SOI) was kept constant to −70 CAD aTDC while sweeping the air-to-fuel ratio.

The results of the combustion parameters obtained from this study are presented in Figure 10. There are no remarkable differences in terms of the combustion parameters. Both the duration and the maximum HRR peak are similar to those of the PFI case. The only substantial difference lies in the maximum pressure reached in the cylinder, which is reasonably lower in the DI case (between 1.5 and 3.5 bar). This effect is attributed to the lower intake pressure required to operate the engine under the same conditions. Since

hydrogen is injected during the compression stroke, no additional work is necessary to force the gas into the cylinder, reducing the demand on the boosting system.

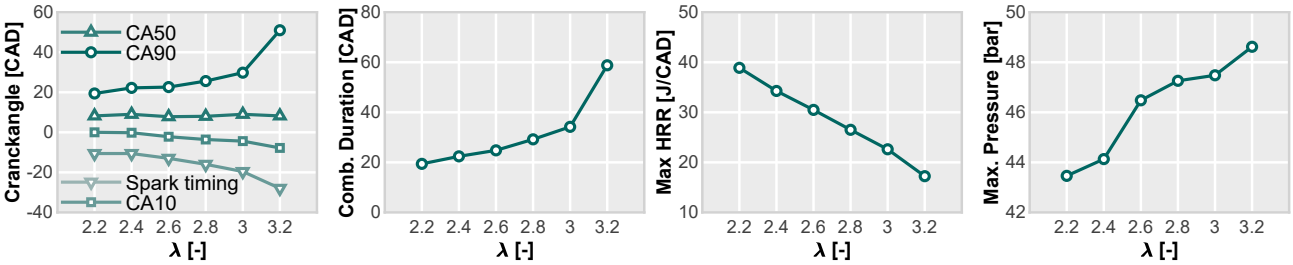

Figure 10. Maximum in-cylinder pressure and HRR peaks, characteristic combustion periods (CA10, CA50, and CA90), spark timing and combustion duration obtained at 1500 rpm engine speed and low-load conditions for various dilution conditions. The results were obtained using the DI system and the SOI was maintained at −70 CAD aTDC in all tests.

Figure 11 shows the impact of the DI system on the engine performance and the NO_x emissions. As can be seen, the main difference is focused on the thermal efficiency and subsequently the specific fuel consumption levels achieved. While the maximum GIE levels for PFI are around 40%, they increase up to 42.5% when using DI. This results in 4 g/kWh of ISFC gain, decreasing up to 70 g/kWh in the low-load case. However, the degree of dilution at which these values are reached is slightly lower. In the case of PFI, the maximum GIE is centered around lambda 3, whereas this value decreases to 2.6 in DI. This is a direct consequence of the deterioration of the combustion stability as the dilution increases in the combustion chamber. In the case of DI, the combustion stability deteriorates earlier with lower degrees of dilution. Note that the combustion duration is remarkably larger for DI (Figure 10) than PFI (Figure 3 at λ = 3.2).

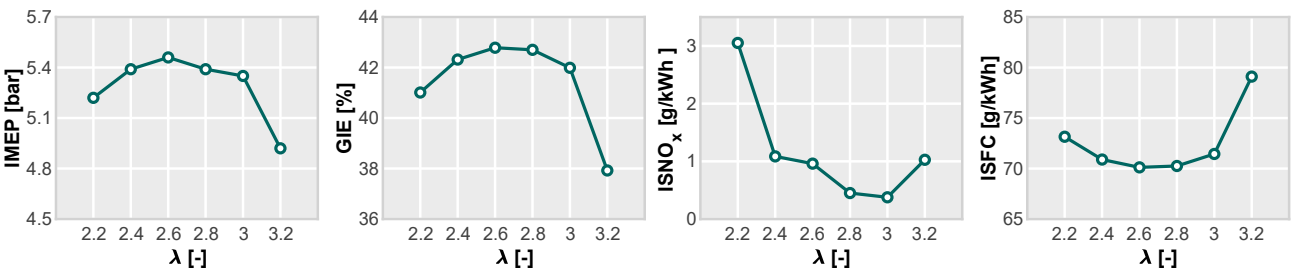

Figure 11. IMEP, GIE, COV_{IMEP}, ISFC and $ISNO_x$ at 1500 rpm engine speed, under low-load conditions and different dilution conditions. Results obtained using the DI system maintaining the SOI at −70 CAD aTDC in all tests.

This effect could be attributed to the interaction of the hydrogen jet and the flow movement inside the combustion chamber. The coupling between these two flows determines the level of turbulence in the chamber and the degree of mixture stratification, both of which are crucial factors in combustion stability and pollutants generation. Low levels of turbulence, resulting from a negative interaction between the tumble motion and the H_2 jet, can potentially lead to unfavorable flame propagation conditions, culminating in a partial or complete misfire. Likewise, the injection timing (SOI) dictates the duration for the hydrogen to achieve homogeneity within the cylinder. Variations in the local λ within the combustion chamber contribute to elevated flame temperatures and augmented NO_x production.

In Figure 12, we depict the main engine performance parameters while varying the SOI and maintaining a constant air-to-fuel ratio (λ = 2.6). Two distinct trends can be discerned associated with the timing of the intake valve closing event. With injection before IVC, the engine performance exhibits minimal fluctuations with SOI retardation. The thermal

efficiency hovers around 40%, and the CCV remains consistently below or close to 1%, underscoring the noteworthy operational stability.

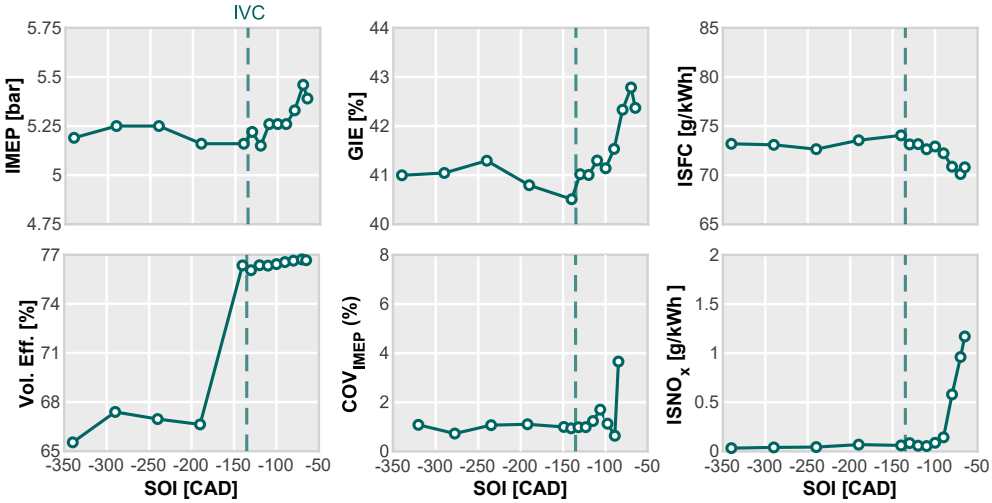

Figure 12. IMEP, GIE, COV_{IMEP}, ISFC, volumetric efficiency and $ISNO_x$ emissions for an engine speed of 1500 rpm, low-load, and λ = 2.6. Combustion phasing was optimized to MBT conditions, and SOI was varied. The dashed line represents the IVC position. Results are from the DI system.

Delaying the SOI results in a substantial enhancement in the engine performance after IVC. The GIE increases from 40% to nearly 43%, accompanied by CCV levels consistently below 1–2% (SOI = −70 CAD aTDC). Consequently, the IMEP experiences an increment, and the ISFC decreases to 70 g/kWh. However, a notable instability peak emerges when the injection initiates at −65 CAD aTDC. At this juncture, the CCV escalates to 4%, and the GIE exhibits a slight decline, indicating that the zenith of performance has been attained. Nevertheless, what remains intriguing is what the graph conceals. The subsequent SOI (−60 CAD aTDC) could not be assessed due to elevated CCV, jeopardizing the operational stability due to an excess of misfiring cycles. This underscores the influence of critical factors, such as the mixing preparation, the flow velocity field, and the turbulence levels within the combustion chamber, which are adversely impacted by delayed injection and contribute to a decline in the combustion stability.

It is evident that NO_x emissions consistently maintain low levels across the majority of the SOI sweep, primarily attributed to the suppressive influence of elevated dilution rates on NO_x formation via the thermal mechanism. However, when the injection timing is further delayed beyond −110 CAD aTDC under low-load conditions, a discernible rise in NO_x emissions becomes apparent. This trend signifies the initiation of a stratified charge, wherein a locally enriched mixture forms, resulting in elevated flame temperatures and consequently augmented NO_x production.

5. Conclusions

The study investigates the viability of hydrogen as a sustainable energy source and its compatibility with internal combustion engines by comparing different operating strategies in a single-cylinder spark-ignition engine. The assessment of the emission levels, the performance, and the combustion characteristics was carried out under varying conditions of dilution, load, and injection timing.

The control of the dilution rate has proven to be a crucial aspect in the quest for higher thermal efficiency while minimizing NO_x emissions. Nevertheless, it is critical not to exceed the dilution limits that could compromise the combustion stability.

The combustion sensitivity to the onset of combustion, and consequently, to the combustion phasing, is another aspect that can aid in the transition to hydrogen-based internal combustion engines. The results have shown that as dilution increases, the range

of stable combustion narrows, which compromises the flexibility of control strategies aimed at improving the driveability and after-treatment system operation.

The direct injection system has demonstrated a significant capability to enhance the engine thermal efficiency (showing an improvement of up to 2 percentage points). Furthermore, when combined with dilution strategies, it enables the control of NO_x emissions by relaxing the boosting system requirements. However, it has become evident that there is a need to optimize the coupling between the chamber design and the injector to maximize the overall system performance.

In summary, this study offers valuable insights into the potential of hydrogen as an alternative fuel for internal combustion engines and underscores important avenues for future research. For example, the sizing and technology of the boosting system and understanding the mixture formation and flow interaction in direct injection combustion chambers are essential considerations.

Author Contributions: Conceptualization, R.N. and J.G.-S.; methodology, J.G.-S.; validation, J.G.-S. and M.O.-G.; formal analysis, J.G.-S. and M.O.-G.; investigation, J.G.-S. and M.O.-G.; resources, S.M. and R.N.; writing—original draft preparation, J.G.-S. and M.O.-G.; writing—review and editing, J.G.-S.; supervision, J.G.-S.; project administration, R.N.; funding acquisition, S.M. All authors have read and agreed to the published version of the manuscript.

Funding: This research has been partially funded by Agencia Estatal de Investigación of the Spanish Government through projects PID2020-118387RB-C31 (AHEAD) and TED2021-130596B-C21 (BIOH2FUEL). M. Olcina-Girona is partly supported by the grant CIACIF/2021/437 of the "Subvenciones para la contratación de personal investigador predoctoral (ACIF)" of the Conselleria d'Innovació, Universitats, Ciència i Societat Digital de la Generalitat Valenciana.

Institutional Review Board Statement: Not applicable.

Informed Consent Statement: Not applicable.

Data Availability Statement: The data presented in this study are available on request from the corresponding author. The data are not publicly available due to privacy.

Acknowledgments: The authors would like to express their gratitude to BORGWARNER for generously providing the medium pressure hydrogen injector. The authors wish to thank Gabriel Alcantarilla for his inestimable assistance during the experimental campaign.

Conflicts of Interest: The authors declare no conflict of interest. The funders had no role in the design of the study; in the collection, analyses, or interpretation of data; in the writing of the manuscript; or in the decision to publish the results.

Abbreviations

The following abbreviations are used in this manuscript:

aTDC	After top dead center
BEV	Battery electric vehicle
CA10	Combustion after 10% of fuel burnt
CA50	Combustion after 50% of fuel burnt
CA90	Combustion after 90% of fuel burnt
CAD	Crank angle degrees
CCV	Cycle-to-cycle variation
CR	Compression ratio
CO	Carbon monoxide
CO_2	Carbon dioxide
COV_{IMEP}	IMEP coeficient of variation
DI	Direct injection
EVC	Exhaust valve closing
EVO	Exhaust valve opening
EU	European Union

FC	Fuel cell
GIE	Gross indicated efficiency
GHG	Greenhouse gases
H_2	Hydrogen
HC	Unburned hydrocarbons
H_2-ICE	Hydrogen internal combustion engine
H_2O	Water
HRR	Heat release rate
ICE	Internal combustion engine
IMEP	Indicated mean effective pressure
ISFC	Indicated specific fuel consumption
$ISNO_x$	Indicated specific NO_x
IVO	Intake valve opening
IVC	Intake valve closing
MBT	Maximum brake torque
NH_3	Ammonia
NO	Nitrogen oxide
NO_2	Nitrogen dioxide
NO_x	Nitrogen oxides
PFI	Port fuel injection
RON	Research octane number
SCR	Selective catalytic reduction
SMR	Steam methane reforming
SI	Spark-ignition
ST	Spark timing
SOI	Start of injection
TDC	Top dead center

References

1. Fuel Cells and Hydrogen Joint Undertaking (FCH). *Hydrogen Roadmap Europe: A Sustainable Pathway for the European Energy Transition*; Publications Office of the European Union: Luxembourg, 2019; p. 70.
2. German Environment Agency. *Fact Sheet: EU 2050 Strategic Vision "A Clean Planet for All" Brief Summary of the European Commission Proposal*; German Environment Agency: Dessau-Roßlau, Germany, 2018.
3. Förster, R.; Kaiser, M.; Wenninger, S. Future vehicle energy supply—Sustainable design and operation of hybrid hydrogen and electric microgrids. *Appl. Energy* **2023**, *334*, 120653. [CrossRef]
4. Dong, Y.; Zheng, W.; Cao, X.; Sun, X.; He, Z. Co-planning of hydrogen-based microgrids and fuel-cell bus operation centers under low-carbon and resilience considerations. *Appl. Energy* **2023**, *336*, 120849. [CrossRef]
5. Danieli, P.; Lazzaretto, A.; Al-Zaili, J.; Sayma, A.; Masi, M.; Carraro, G. The potential of the natural gas grid to accommodate hydrogen as an energy vector in transition towards a fully renewable energy system. *Appl. Energy* **2022**, *313*, 118843. [CrossRef]
6. Ishaq, H.; Dincer, I.; Crawford, C. A review on hydrogen production and utilization: Challenges and opportunities. *Int. J. Hydrogen Energy* **2022**, *47*, 26238–26264. [CrossRef]
7. Serrano, J.; Martín, J.; Gómez-Soriano, J.; Raggi, R. Theoretical and experimental evaluation of the spark-ignition premixed oxy-fuel combustion concept for future CO_2 captive powerplants. *Energy Convers. Manag.* **2021**, *244*, 114498. [CrossRef]
8. Desantes, J.; Molina, S.; Novella, R.; Lopez-Juarez, M. Comparative global warming impact and NO_X emissions of conventional and hydrogen automotive propulsion systems. *Energy Convers. Manag.* **2020**, *221*, 113137. [CrossRef]
9. Novella, R.; De la Morena, J.; Lopez-Juarez, M.; Nidaguila, I. Effect of differential control and sizing on multi-FCS architectures for heavy-duty fuel cell vehicles. *Energy Convers. Manag.* **2023**, *293*, 117498. [CrossRef]
10. Yun, H.; Bu, Z.; Yang, Z.; Wang, L.; Zhang, B. Optimization of fuel injection timing and ignition timing of hydrogen fueled SI engine based on DOE-MPGA. *Int. J. Hydrogen Energy* **2023**, *48*, 9462–9473. [CrossRef]
11. Shi, C.; Chai, S.; Wang, H.; Ji, C.; Ge, Y.; Di, L. An insight into direct water injection applied on the hydrogen-enriched rotary engine. *Fuel* **2023**, *339*, 127352. [CrossRef]
12. Yip, H.L.; Srna, A.; Yuen, A.C.Y.; Kook, S.; Taylor, R.A.; Yeoh, G.H.; Medwell, P.R.; Chan, Q.N. A review of hydrogen direct injection for internal combustion engines: Towards carbon-free combustion. *Appl. Sci.* **2019**, *9*, 4842. [CrossRef]
13. Verhelst, S.; Wallner, T. Hydrogen-fueled internal combustion engines. *Prog. Energy Combust. Sci.* **2009**, *35*, 490–527. [CrossRef]
14. Xie, S.; Chen, X.; Wang, Y.; Zhang, T.; Chen, Z. Numerical study on forced ignition and flame propagation in a counterflow of nitrogen-diluted hydrogen versus air. *Fuel* **2024**, *357*, 129863. [CrossRef]
15. WG, P.K.; Ranjith, P. An overview of underground hydrogen storage with prospects and challenges for the Australian context. *Geoenergy Sci. Eng.* **2023**, *231*, 212354.

16. Khristamto Aditya Wardana, M.; Lim, O. Investigation of ammonia homogenization and NOx reduction quantity by remodeling urea injector shapes in heavy-duty diesel engines. *Appl. Energy* **2022**, *323*, 119586. [CrossRef]
17. Bao, L.Z.; Sun, B.G.; Luo, Q.H. Experimental investigation of the achieving methods and the working characteristics of a near-zero NOx emission turbocharged direct-injection hydrogen engine. *Fuel* **2022**, *319*, 123746. [CrossRef]
18. Bao, L.Z.; Sun, B.G.; Luo, Q.H. Optimal control strategy of the turbocharged direct-injection hydrogen engine to achieve near-zero emissions with large power and high brake thermal efficiency. *Fuel* **2022**, *325*, 124913. [CrossRef]
19. Bao, L.Z.; Sun, B.G.; Luo, Q.H.; Li, J.C.; Qian, D.C.; Ma, H.Y.; Guo, Y.J. Development of a turbocharged direct-injection hydrogen engine to achieve clean, efficient, and high-power performance. *Fuel* **2022**, *324*, 124713. [CrossRef]
20. Barış, O.; Güler, I.; Yaşgül, A. The effect of different charging concepts on hydrogen fuelled internal combustion engines. *Fuel* **2023**, *343*. [CrossRef]
21. Park, C.; Lee, S.; Kim, C.; Choi, Y. A comparative study of lean burn and exhaust gas recirculation in an HCNG-fueled heavy-duty engine. *Int. J. Hydrogen Energy* **2017**, *42*, 26094–26101. [CrossRef]
22. Gao, J.; Wang, X.; Song, P.; Tian, G.; Ma, C. Review of the backfire occurrences and control strategies for port hydrogen injection internal combustion engines. *Fuel* **2022**, *307*, 121553. [CrossRef]
23. Shen, Q.; Wang, G.; Wang, Y.; Zeng, B.; Yu, X.; He, S. Prediction Model for Transient NOx Emission of Diesel Engine Based on CNN-LSTM Network. *Energies* **2023**, *16*, 5347. [CrossRef]
24. Verhelst, S. Recent progress in the use of hydrogen as a fuel for internal combustion engines. *Int. J. Hydrogen Energy* **2014**, *39*, 1071–1085. [CrossRef]
25. Koch, D.T.; Eßer, E.; Kureti, S.; Sousa, A. H2-deNOx catalyst for H2 combustion engines. *MTZ Worldw.* **2020**, *81*, 30–35. [CrossRef]
26. Thawko, A.; Persy, S.A.; Eyal, A.; Tartakovsky, L. Effects of Fuel Injection Method on Energy Efficiency and Combustion Characteristics of SI Engine Fed with a Hydrogen-Rich Reformate. *SAE Tech. Pap.* **2020**, 1–12. [CrossRef]
27. Molina, S.; Ruiz, S.; Gomez-Soriano, J.; Olcina-Girona, M. Impact of hydrogen substitution for stable lean operation on spark ignition engines fueled by compressed natural gas. *Results Eng.* **2023**, *17*, 100799. [CrossRef]
28. Molina, S.; Novella, R.; Gomez-Soriano, J.; Olcina-Girona, M. Study on hydrogen substitution in a compressed natural gas spark-ignition passenger car engine. *Energy Convers. Manag.* **2023**, *291*, 117259. [CrossRef]
29. Payri, F.; Olmeda, P.; Martin, J.; Carreño, R. A New Tool to Perform Global Energy Balances in DI Diesel Engines. *SAE Int. J. Engines* **2014**, *7*, 43–59. [CrossRef]
30. Sagar, S.; Agarwal, A.K. Knocking behavior and emission characteristics of a port fuel injected hydrogen enriched compressed natural gas fueled spark ignition engine. *Appl. Therm. Eng.* **2018**, *141*, 42–50. [CrossRef]

Disclaimer/Publisher's Note: The statements, opinions and data contained in all publications are solely those of the individual author(s) and contributor(s) and not of MDPI and/or the editor(s). MDPI and/or the editor(s) disclaim responsibility for any injury to people or property resulting from any ideas, methods, instructions or products referred to in the content.